Crystallization and mechanical behavior of the ferroelectric polymer nonwoven fiber fabrics for highly durable wearable sensor applications

Z.H. Liu [a,b,c,d], C.T. Pan [a,b,c,*], C.K. Yen [a,b,c], L.W. Lin [e,f], J.C. Huang [g], C.A. Ke [a]

[a] Department of Mechanical and Electro-Mechanical Engineering, National Sun Yat-Sen University, Kaohsiung 80424, Taiwan
[b] Center for Nanoscience & Nanotechnology, National Sun Yat-Sen University, Taiwan
[c] National Science Council Core Facilities Laboratory for Nano-Science and Nano-Technology in Kaohsiung-Pingtung Area, Taiwan
[d] Micro/Meso Mechanical Manufacturing R&D Department, Metal Industries Research and Development Centre, Kaohsiung 81160, Taiwan
[e] Department of Mechanical Engineering, University of California, Berkeley, CA 94720, United States
[f] Berkeley Sensor and Actuator Center, University of California, Berkeley, CA 94720, United States
[g] Department of Materials and Optoelectronic Science, National Sun Yat-Sen University, Kaohsiung, Taiwan

ARTICLE INFO

ABSTRACT

The mechanical characterization of the electrospinning polyvinylidene fluoride (PVDF) nonwoven fiber fabrics (NFFs) doped with multi-walled carbon nanotubes (MWCNTs) was investigated. Piezoelectric composite nanofibers of the PVDF/MWCNTs were directly electrospun by the hollow cylindrical near-field electrospinning (HCNFES) without any post-poling treatment. We have made the HCNFES NFFs consisted of high-orderly arranged nanofiber assemblies for further characterizing the effect of MWCNTs filling PVDF nanofibers. An *in situ* electrical poling and high uniaxial stretching imparted on the polymer jet during the HCNFES process, which naturally align the dipoles in the PVDF crystals and promote the formation of the polar β-crystalline phase within the fibers. Moreover, the reinforcement of the HCNFES PVDF nanofibers indicated the improvement in mechanical properties and the degree of high oriented extended-chain crystallites through adding adequate contents of MWCNTs. In the case of alignment of the all-trans polymer chains in the vicinity of MWCNTs along the fiber axis, X-ray diffraction (XRD) patterns showed the strongest diffraction peak of the β-crystalline phase. In the comparison of the near-field electrospinning (NFES), the HCNFES nanofibers with smooth surface and smaller diameter can easily form high density structural NFFs. After nano-indentation and tensile strength measurements, the results indicated that the mechanical properties of the HCNFES NFFs are better than the NFES ones. When 16 wt% PVDF solution doped with 0.03 wt% MWCNTs, the results reveal that Young's modulus, hardness, yield stress, yield strain, ultimate tensile strength, and strain at break of the HCNFES composite NFFs are obviously enhanced to 1.39 GPa, 39.6 MPa, 28 MPa, 48.17 MPa, 3.3%, and 32.5%, respectively. Finally, a flexible wearable sensor made of three-dimensional piezoelectric NFFs was actually experimented. Outstanding mechanical properties with highly deformable of PVDF/MWCNTs composite nanofibers would maintain it to represent great challenges during practical implementation.

© 2015 Elsevier B.V. All rights reserved.

1. Introduction

Recent developments in the field of the fabrication of one-dimensional ferroelectric fibers have attracted much attention and opened up tempting opportunities. Nanoengineering has enabled researchers and engineers to fabricate nanomaterials to construct lots of nanostructures for a wide range of utilization. One-dimensional piezoelectric nanofibers and nanotubes fabricated by lead zirconate titanate (PZT) [1–4], zinc oxide (ZnO) [5–9], and PVDF [10–13] have shown considerable progress for various potential applications such as energy scavengers, sensors, and electromechanical actuators. In order to get a good performance, the evaluation of their mechanical properties is more important. Therefore, in this article, we have aimed to mechanically characterize the multi-walled carbon nanotubes (MWCNTs) reinforced

* Corresponding author at: Department of Mechanical and Electro-Mechanical Engineering, National Sun Yat-Sen University, No. 70 Lien-hai Road, Kaohsiung 80424, Taiwan. Tel.: +886 7 5252000x4239; fax: +886 7 5254299.
   E-mail address: panct@mail.nsysu.edu.tw (C.T. Pan).

Table 1
Experimental data of PVDF solutions used in this study, including weight percentage of PVDF powder, solvent, surfactant, and MWCNTs.

PVDF powder		Solvent (DMSO:acetone)		Surfactant (Zonyl®UR)		MWCNTs	
Weight ratio (PVDF/solvent) (wt%)	Weight (g)	DMSO (g)	Acetone (g)	Weight ratio (wt%)	Weight (g)	Weight ratio (wt%)	Weight (g)
16	0.8	2.5	2.5	5	0.25	0	0
18	0.9	2.5	2.5	5	0.25	0	0
20	1	2.5	2.5	5	0.25	0	0
16	0.8	2.5	2.5	5	0.25	0.03	0.015
16	0.8	2.5	2.5	5	0.25	0.05	0.025

electrospun PVDF nonwoven fiber fabrics (NFFs) fabricated by the hollow cylindrical near-field electrospinning (HCNFES) and the near-field electrospinning (NFES) processes. It has been found that the nano-indentation and tensile strength tests provided an assessment of average mechanical properties of the PVDF NFFs rather than measuring an individual nanofiber for further flexible wearable sensor applications.

PVDF nanomaterials are attractive in low-cost, processability, high resistance to fatigue, chemical resistance, thermal stability, and environmentally friendly applications [14]. PVDF is a semicrystalline ferroelectric polymer with high molecular weight and typically has around 50% amorphous content. This polymer can crystallize into four different crystal forms, α, β, γ, and δ. The α phase consists of TGTG (alternating trans gauche) conformations, while the β phase consists of the all-trans (TTTT) planar zigzag conformation. Among these structures, β phase is expected to display a stronger piezoelectric response, which has been discovered to induce polarity in the crystal structures. During electrospinning processes, the oriented β-form extended-chain crystallites can be formed. The suggested mechanisms are that *in situ* electric poling and mechanical stretching throughout orderly arranged electrospinning processes, which could drive the dipoles to reorganize in the same direction. For the purpose of producing the polar β-crystalline phase in PVDF fibers, high electrical field, strong polymer stretching, high pressure and annealing were required during the manufacturing processes to align the dipoles in the crystalline structures [15–19]. Yee et al. presented the far-field electrospinning (FFES) on a rotating disk to collect electrospun fibers [20]. In a typical electrospinning process (tip-to-collector distance in the range of 30–150 mm; bias: 10–20 kV; electrical field strength: $0.8–3.3 \times 10^5$ V/m) [10,21], the droplet of the polymer solution at the needle tip was distorted into a cone under a high electric bias voltage. After the charged droplet overcame its own viscoelasticity and surface tension, the solution jet were emitted from a Taylor cone, and subsequently electrostatic force stretched the semi-solidified fiber into an involved route, causing fiber into chaotic whipping. The fibers were almost randomly oriented, such as in the directions of upward, downward or parallel to collectors. However, the dipole moments in these fibers would lead to offset each other, revealing worse piezoelectric properties than orderly ones.

The NFES [22,23] and HCNFES processes [24] were proposed to improve those problems to strengthen the fiber controllability such as diameter, structural features and density, and internal crystallinity. Moreover, field strength $\sim 10^5$ V/m for electric poling is too low, and a thin polymer sheet has been suggested to replace air gap to enhance effectively electric field poling process. By contrast, the NFES and HCNFES processes, tip-to-collector distance can reduce to several millimeters and enhance the degree of electric field (tip-to-collector: 0.5–2 mm; bias: 0.8–16 kV; field strength: $10^6–10^7$ V/m). Unlike the FFES process, the two modified electrospinning processes only need a small electric bias voltage to produce controllable fiber deposition, nearly an order of magnitude lower than conventional near-field electrospinning.

In addition, for performing further applications, the mechanical characterization of electrospun fibers or fibrous structures would be essential to know if they were strong enough to resist the external and internal forces. Gu et al. [25], by attaching a single fiber to an atomic force microscopy cantilever; the measurement of the Young's modulus of electrospun polyacrylonitrile fiber was reported. The force–displacement curves obtained by the bending of a single fiber used to calculate the Young's modulus. Tang and Liu [26] discussed the mechanical properties of polyvinyl alcohol composite film reinforced with high volume of electrospun cellulose nanofibrous mat. Compared with neat polyvinyl alcohol film, the mechanical strength and Young's modulus of composites were increased. The relationship between the extensional force and the formation of oriented crystallites in the electrospun PVDF composite fibers was reported by Huang et al. [27]. The characterization of crystal orientation of the FFES PVDF/CNTs fibers revealed that the interfacial interaction between the CNTs and PVDF chains can perform synergistically to facilitate the nucleation of oriented β-form extended-chain crystallites at the interface.

We utilize a direct-write technique by means of the HCNFES to produce the well-controlled deposition of piezoelectric PVDF/MWCNTs nanofibers and NFFs. Under high *in situ* electrical poling, elongation, and high-speed mechanical stretching during electrospinning process, the surface morphology and internal crystallization of the NFFs were demonstrated by scanning electron microscopy (SEM) and X-ray diffraction (XRD), respectively. The HCNFES PVDF nanofibers with smaller diameters, smooth surface and great crystallinity have been manufactured into a prototype of highly durable flexible wearable sensing device, required for subsequently applications in protection from exercise injuries and long-term care.

2. Materials and methods

The formation of electrospun fibrous structures depends on the construction and geometrical shape of the electrospinning machine set-up. The characteristics of the HCNFES process is shown in Fig. 1(a), which includes a stainless needle, infusion pump, high voltage power supply, X–Y control platform. A rotating glass tube collector is used to collect electrospun PVDF nanofibers. Copper foil is stuck in internal wall surface of the glass tube for grounding via an electrode brush. Bias voltage creates high electric field between the needle tip and the grounded tube collector. To control uniaxial movement and rotation of the tube collector, the programmable X–Y control platform and DC motor are used. Fig. 1(b) shows the working principle of the NFES process [22,23].

Table 1 lists the details and records in various PVDF solutions in this work. The amount of solution is prepared about 6 g (solvent 5 g). The concentration of all substances is calculated in weight ratio (wt%). To reduce surface tension of the PVDF solutions for stably electrospinning PVDF nanofibers, adding the surfactant (Zonyl®UR) can induce polymer jet formation due to its ionic character [29], resulting in increasing the conductivity of the PVDF solutions. In addition, CNTs have been reported to act as the nucleating agent
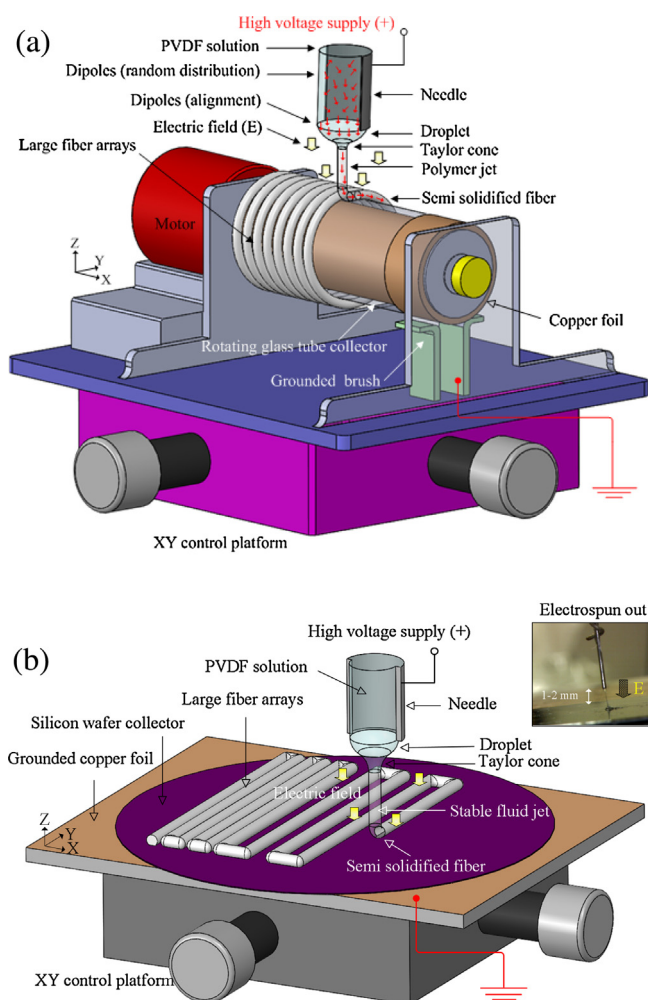
Fig. 1. (a) Schematic illustration of the HCNFES process and direct-write PVDF nanofibers with ultra-long length and large area on the rotating glass tube collector. The random distribution of dipoles in PVDF solution can transfer into alignment of dipoles when the semi-solidified PVDF fiber is electrospun on the collector. Moreover, the tangential force induces a mechanical stretching between glass tube collector and semi-solidified PVDF fibers, resulting in alignment of dipoles along longitudinal direction and (b) schematic diagram of the NFES process. The collector is mounted on a controllable stage. After the semi-solidified PVDF fiber suffers *in situ* electrical poling and mechanical stretching, PVDF nanofibers orderly pattern on the collector.

for polymer crystallization as well as the template for polymer chain orientation [30–33]. In our earlier research [11,34], diameter of the PVDF nanofibers can be adjusted by controlling various parameters such as internal diameter of needle, electric field, tangential speed on collector surface, PVDF solution concentration, and MWCNTs concentration. The results showed that when the internal diameter of needle is bigger than 0.26 mm, the initial droplet would excessively accumulate on the need tip, leading to directly drop on collectors, and subsequently blocking spinning route. By contrast, as the needle size was too thin, the PVDF solutions were difficult to electrospin out due to high viscous resistance on internal wall of needles. In continuous HCNFES and NFES processes setup, electric bias voltage can be manipulated to directly control the diameter of nanofibers. Operation at such low voltages effectively reduces the fiber deposition in disorganized and disorderly collection, which enables deposition of the ultra-thin PVDF nanofibers. However, insufficient electrical field strength would provide poor polarization results, but excessive bias voltage would cause short circuit, resulting in discontinuity of the electrospinning processes. In addition, the fiber diameter was inversely proportional to tangential speed. At excessively low tangential speed, the fiber ejection rate exceeded the collection rate, resulting in disorganized and disorderly collection. At excessively high tangential speed, the fiber collection rate exceeded the ejection rate, resulting in disruption and discontinuous collection. Therefore, the balance between fiber ejection rate and collection rate is more important for further large deposition of the NFFs.

After that, the parameters of various PVDF solutions for electrospinning process were prepared using the following steps: (1) dimethyl sulfoxide (DMSO) used as the solvent for PVDF powder (Mw = 534,000), with fluorosurfactant (ZONYL®UR) and acetone to reduce the surface tension and improve the evaporation rate of PVDF solution, respectively; (2) for developing high-performance PVDF/MWCNTs nanofibers, the proper percentage of MWCNTs was dispersed in DMSO via sonication dispersion method; and (3) two solutions of PVDF and MWCNTs-DMSO were mixed and stirred until forming a homogenous PVDF/MWCNTs solution. The formation of electrospun PVDF NFFs consisted of nanofiber arrays layer-by-layer assembly via accurately programming loops of the collectors. For the purpose of producing a stable jet of polymer solution during the HCNFES process [24], needle size of 0.26 mm, flow rate of syringe pump setting at 0.001 ml/min, *X–Y* platform speed of 2 mm/s, rotating velocity of 900 rpm with tangential speed on tube surface of 942.5 mm/s, electric field of 1×10^7 V/m were set.
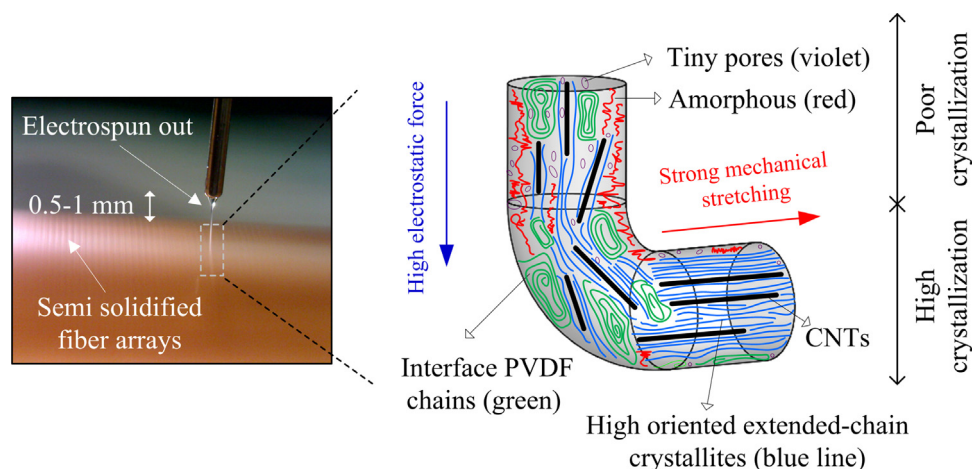

Fig. 2. The enlarged view shows the high oriented extended-chain crystallites (blue lines), interface PVDF chains (green), amorphous (red), and tiny pores (violet) in the formation of the HCNFES composites nanofibers. (For interpretation of the references to color in this figure legend, the reader is referred to the web version of the article.)
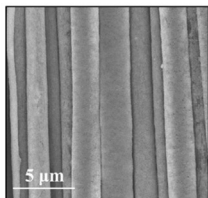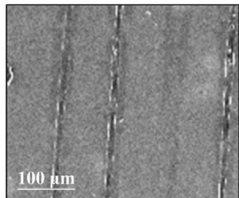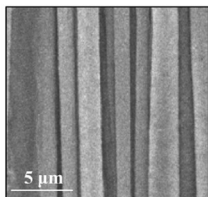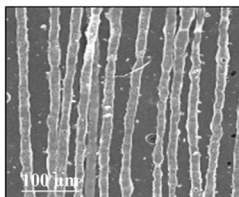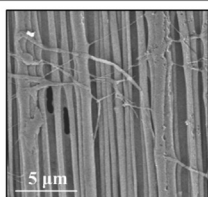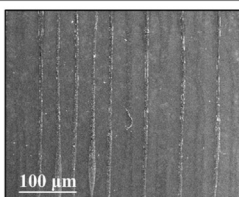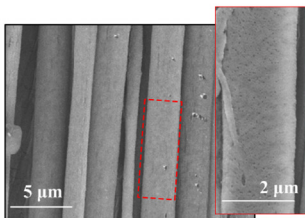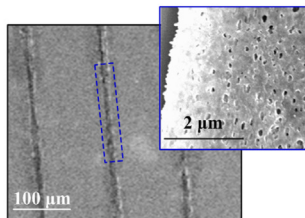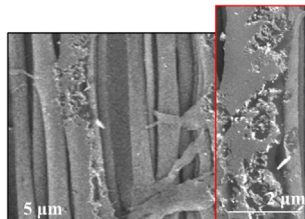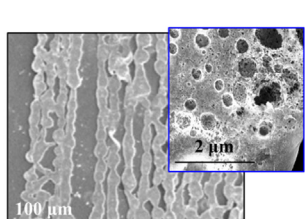
	HCNFES nanofiber arrays	Diameter	NFES nanofiber arrays	Diameter
16%wt PVDF	(a1)	2 μm ≀ 2.5 μm	(b1)	13 μm ≀ 20 μm
18%wt PVDF	(a2)	1.2 μm ≀ 2 μm	(b2)	10 μm ≀ 20 μm
20%wt PVDF	(a3)	0.7 μm ≀ 1 μm	(b3)	5 μm ≀ 9 μm
16%wt PVDF +0.03%wt MWCNT	(a4)	0.5 μm ≀ 2.5 μm	(b4)	~10 μm
16%wt PVDF +0.05%wt MWCNT	(a5)	~ 2.5 μm	(b5)	~15 μm

Fig. 3. SEM micrographs of the HCNFES NFFs and the NFES PVDF nanofiber arrays with doping different weight ratios of MWCNTs. The HCNFES PVDF NFFs: (a₁) 16 wt% PVDF; (a₂) 18 wt%; (a₃) 20 wt%; (a₄) 16 wt% + 0.03 wt% MWCNT; (a₅) 16 wt% + 0.05 wt% MWCNT. The NFES PVDF fiber arrays: (b₁) 16 wt% PVDF; (b₂) 18 wt% PVDF; (b₃) 20 wt%; (b₄) 16 wt% + 0.03 wt% MWCNT; (b₅) 16 wt% + 0.05 wt% MWCNT.

In the NFES process, X–Y platform speed was 70 mm/s, and electric field was also fixed at 1×10^7 V/m.

2.1. Electrospinning induced ferroelectricity in the PVDF nanofibers

Fig. 2 shows the suggested mechanism for the formation of high oriented extended-chain crystallites, forming in the HCNFES composite nanofibers. In the HCNFES and NFES processes, high electric field is created between the needle tip and the tube collector. When the droplet overcomes the surface tension of the solution, an ultra-thin PVDF fiber is electrospun from the Taylor cone tip. The charged jet is quickly elongated and accelerated by the electric field, and undergoes a variety of instabilities, electric poling, mechanical stretching, and evaporation before orderly fiber deposition. Under a relatively high tangential speed on the tube surface, high-speed stretching can perform ultra-thin PVDF nanofiber deposition with smooth surface. Compared with traditionally electrospinning and NFES processes, the HCNFES technique is able to continuously and rapidly collect the PVDF nanofibers through a great traction on the collector surface, which effectively overcomes the patterning perturbations such as disruption and local spiraling effect in the electrospinning process. Additionally, in the β-form extended-chain crystallites, the electric dipoles paralleling to the polar axis generate between the fluorine atoms to hydrogen atoms in individual molecular chains. These molecular chains generate

the orientation of dipoles and/or ferroelectric domains [28], which can be reversed and oriented through a high electric field in the HCNFES process. Hence, the HCNFES process is expected to reinforce crystallinity and fraction of the polar β-crystalline phase in the ultra-thin PVDF nanofibers.

2.2. Micrograph and crystallinity of the PVDF/MWCNTs NFFs

Fig. 3(a_1)–(a_5) shows SEM photomicrograph of the HCNFES PVDF NFFs and they doped with different weight ratios of MWCNTs. The significant changes in the fiber diameters and surface morphology were observed. Smooth and uniformly deposited NFFs were obtained for the samples 3(a_1)–(a_4). As the solution concentration was lower than 16 wt%, the electrospinning process tended to discontinuous owing to an unsteady solution flow rate. In order to provide the right balance of viscosity and surface tension necessary of the PVDF solution, the concentration of the PVDF solution was controlled at within 16–20 wt% to electrospin stably continuous jet of polymer solution. When the concentration of MWCNTs exceeded 0.05 wt%, the solution was difficult to electrospin because of aggregation, and subsequently caused the fiber diameter distribution to widen and cracks on the fiber surface. Fig. 3(a_4) shows the uniformly deposited NFFs with 0.03 wt% MWCNTs. The enlarged surface morphology of one single nanofiber shows smooth surface that just some tiny pores with the size in the range of 10–50 nm, which can be explained by the evaporation of the volatile acetone in the PVDF solution. The HCNFES nanofibers can control fiber diameter in the range of from 200 nm to few micrometers, length, and structural thickness.

Fig. 3(b_1)–(b_5) shows the SEM photomicrograph of the NFES PVDF fiber arrays with various weight ratios of MWCNTs. The changes of fiber diameter and surface morphology can be observed. Comparing NFES and HCNFES processes, the NFES fibers show a worse surface roughness, especially the defects such as holes and voids can be observed while over-addition of MWCNTs (0.05 wt%). These defects could be in the range of 100–500 nm. In addition to aggregation of MWCNTs, these are caused by a great amount of volatile acetone in the formation of semi-solidified PVDF nanofibers during the NFES process. Under a lower collecting speed (collecting speed of the HCNFES process is large about twenty times to the NFES process), unsteady solution flow rate in the initial NFES process can be observed. Thus, the solvent may not have completely evaporated from the fiber surface, which resulted in tiny holes left on the surface. The nucleation of high oriented extended-chain crystallites in the electrospun nanofibers plays an important critical role in mechanical properties [34]. Fig. 4(a) shows the results from the original PVDF powder before the electrospinning process, and it clearly exhibits strong presence of the α phase with diffraction peaks at 18.8°, and 20.2°, corresponding to the (0 2 0) and (1 1 0). After high *in situ* electrical poling and high-speed mechanical stretching, the HCNFES process would easily align the dipoles and induce more oriented β-form extended-chain crystallites along the fiber axis in the PVDF nanofibers. In this plot, one can observe the diffraction peaks around 20.6°–20.98°, representing the β phase (1 1 0). It is further noted that if the concentration of PVDF exceeded its equilibrium solubility limit (more than 20 wt% PVDF), homogeneous solution would be difficult to achieve, leading to the β phase decrease. As doping 0.03 wt% MWCNT in the PVDF nanofibers, the results show the obviously enhancement of the β phase, and only a very small peak of the α phase can be detected (Fig. 4(a) and (b)). By contrast, after over-addition of MWCNTs (0.05 wt%), the β-phase proportion would decrease. At such high collecting speed in the HCNFES process, perturbations in the fiber deposition owing to bending instabilities are reduced, thereby increasing controllability of the electrospun polymer jet and resulting well aligned nanofibers. In addition, the
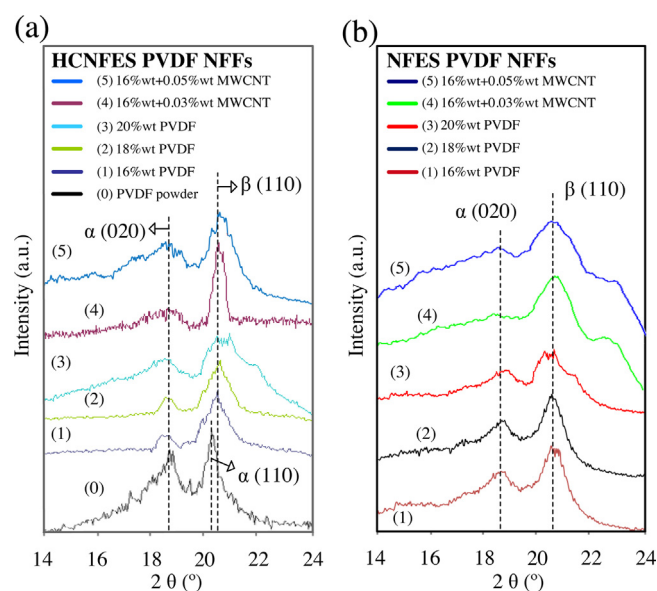

Fig. 4. (a) XRD patterns of the PVDF powder and the HCNFES NFFs with different MWCNT weight ratios and (b) the NFES NFFs with different MWCNT weight ratios.

HCNFES process with a high-speed mechanical stretching not only allows for uniformly the ultra-thin PVDF nanofibers deposition with smooth surface, but also may improve the piezoelectric β-crystalline phase concentration as plotted in XRD results.

3. Mechanical and piezoelectric properties

For a viscoelastic material, in addition to the viscoelastic properties in the time domain, the material properties can also be represented by complex material functions in the frequency domain [35]. In order to gain better understanding of how the electrospun piezoelectric composite NFFs behave, in this section, preliminary mechanical testing is performed by nano-indentation and tensile strength tests [36]. Large amounts of nanofiber arrays were continuously collected and stacked assembly via the HCNFES and NFES processes as the formation of NFFs, which the thickness and areal density are at ranges of ~20 μm (Fig. 3(a)) and ~1000 nanofibers/mm^2, respectively.

3.1. The nano-indentation method

The mechanical properties of the HCNFES and NFES PVDF NFFs were examined using mechanical testing and simulation (MTS) nanoindenter Windows XP system. The elastic modulus and hardness were measured using the continuous stiffness module (CSM) technique. The CSM technique enables the instrument to measure the contact stiffness throughout the experiment. A Berkovich indenter is a three-sided pyramid with an approximately 40 nm tip radius. Nano-indentation testing is used to analyze load–displacement curves and contact area between the NFFs and the indenter to calculate Young's modulus and hardness. This system records the indenter dynamic load–displacement curves during indentation, with load resolution of 50 nN and displacement resolution of 0.01 nm. Under a constant indenter displacement velocity of 20 nm/s, the indenter with a normal force of 2 mN penetrates the NFFs into a depth of 2000 nm. Fig. 5(a) shows the load–displacement curves and SEM microphoto of the cross-sectional view of the PVDF NFFs on a silicon substrate. Fig. 5(b) shows the modulus as a function of depth from the HCNFES NFFs with using 16 wt% PVDF solution and 0.03 wt% MWCNTs. The variation of elastic modulus at shallow depth indentation in the range of
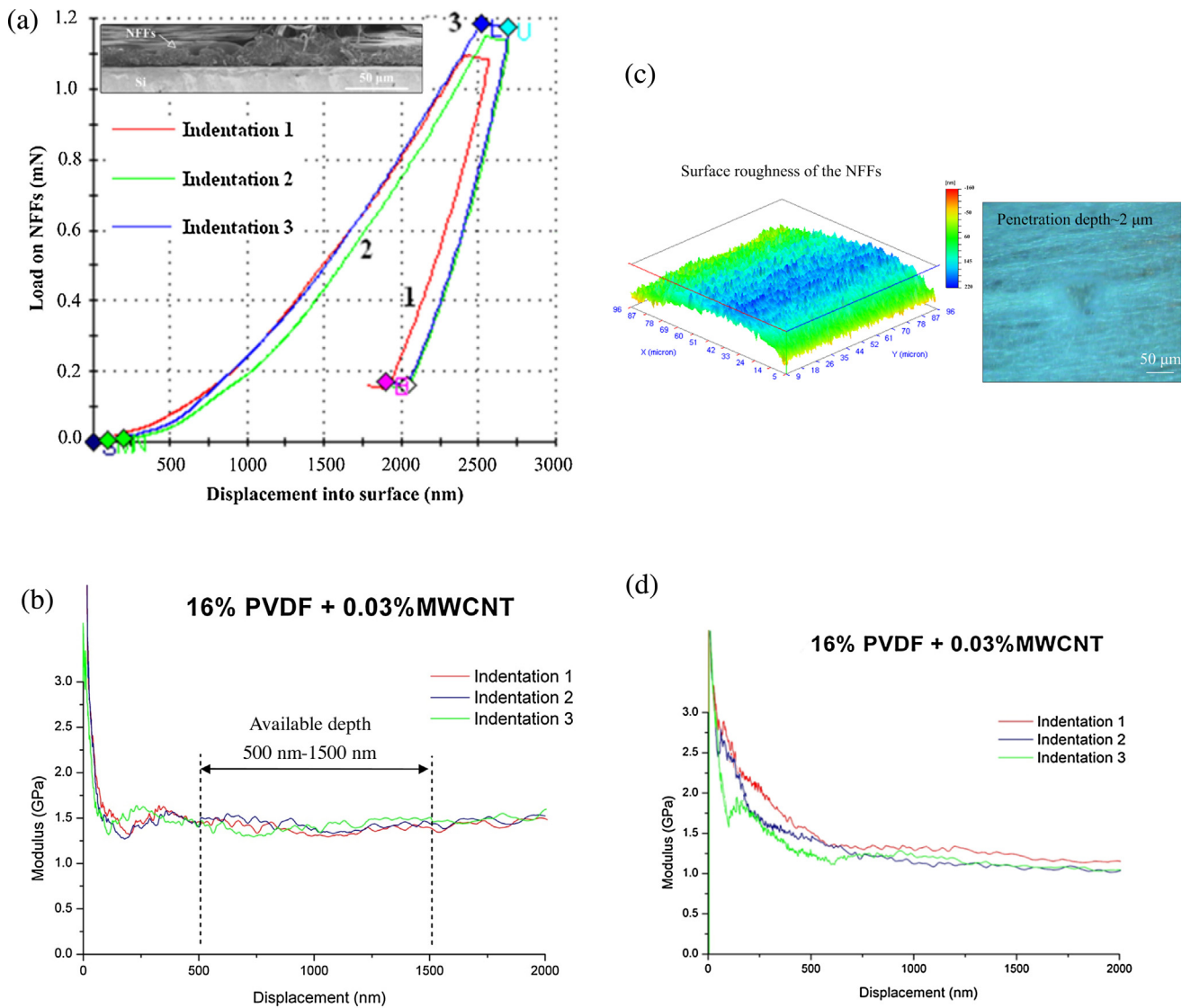
Fig. 5. (a) Load–displacement curves during indentation testing. The modulus of the composite nanofibers with 16 wt% PVDF solution and 0.03 wt% MWCNTs by means of the HCNFES and NFES processs: (b) modulus as a function of depth measured by the HCNFES NFFs; (c) surface roughness of the NFFs and OM image of indentation configuration on the NFFs; (d) modulus as a function of depth measured by the NFES NFFs (each sample has three indentations on the surface).

from surface to 350 nm would cause by the surface roughness and non-ideal tip geometry of the indenter [37]. The surface roughness of the NFFs with roughness in the range of 160–220 nm was scanned by using nanovision. The pyramidal image of the indentation configuration on the NFFs is shown in Fig. 5(c). In the depth of 500–1500 nm, the results show that the modulus is almost stabilized at around ∼1.39 GPa. Fig. 5(d) shows the modulus as a function of depth from the NFES NFFs. The modulus is about 1.22 GPa. In the depth of 350–600 nm, the elastic modulus lightly decreased with the indentation depth. It is suggested that the surface defects

such as tiny holes and voids existing in the NFES NFFs would cause the mechanical properties to down. Table 2 shows average modulus and hardnesses of the NFFs using various solutions via the two electrospinning methods. The modulus is proportional to PVDF solution concentration. When the concentration is lower than 16 wt%, the electrospinning processes become discontinuous because of unsteady solution flow rate, leading to non-uniform fiber diameter. Although the modulus is bigger than the others after the solution concentration exceeds 16 wt%, however, the increasing solution concentration would not get the desired viscosity and

Table 2
Average modulus and hardnesses of the HCNFES and NFES NFFs were calculated based on 10 data points measured directly from Figs. 5 and 6 in each experiment, respectively.

	HCNFES NFFs		NFES NFFs	
	Modulus (GPa)	Hardness (GPa)	Modulus (GPa)	Hardness (GPa)
16 wt% PVDF	0.89	0.026	0.79	0.024
18 wt% PVDF	1.02	0.03	0.91	0.026
20 wt% PVDF	1.17	0.035	1.03	0.029
16 wt% PVDF/0.03 wt% MWCNTs	1.39	0.039	1.22	0.035
16 wt% PVDF/0.05 wt% MWCNTs	1.09	0.033	0.90	0.027

(a) **16% PVDF + 0.03%MWCNT**
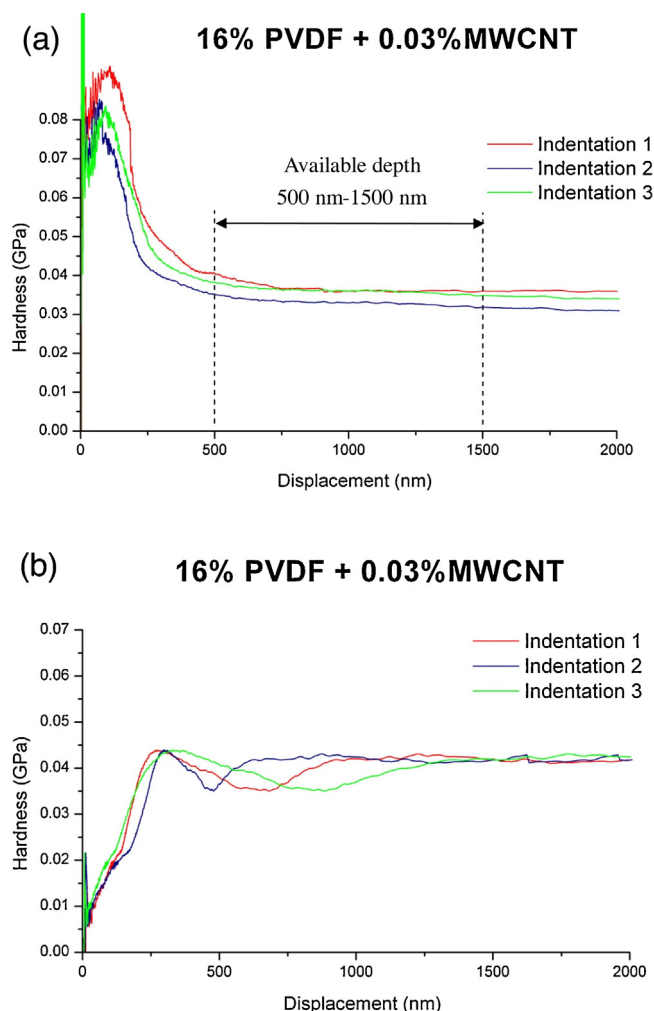

(b) **16% PVDF + 0.03%MWCNT**

Fig. 6. The hardnesses of the NFFs with 16 wt% PVDF solution and 0.03 wt% MWCNTs by the HCNFES and NFES processes: (a) hardness as a function of depth measured by the HCNFES NFFs and (b) hardness as a function of depth measured by the NFES NFFs.

Fig. 7. (a) A photograph shows the schematic diagram of deformation of the electrospun NFFs after tensile test and (b) fracture surface of the electrospun NFFs and the enlarged views of one single nanofiber.

surface tension property for producing a *stable jet* of *polymer* solution. In addition, the nucleation of highly oriented extended-chain crystallites in the electrospinning nanofibers induced by the interactions between MWCNTs and polymer crystallites was expected to have a great mechanical properties [33]. After doping 0.03 wt% of MWCNTs in the PVDF NFFs, apparently the modulus increased. Nevertheless, when MWCNTs in PVDF solution exceeds 0.05 wt%, the electrospun NFFs would grow lots of cracks on the fiber surface due to aggregation of MWCNTs, leading to poor crystallization and decrease in modulus. These phenomena were further confirmed by the SEM results and XRD patterns shown in Figs. 3 and 4, respectively. The hardness as a function of depth from the HCNFES NFFs with 16 wt% PVDF solution and 0.03 wt% MWCNTs is shown in Fig. 6(a). The results shows that the hardness is about 0.039 GPa. The hardness of the NFFs is nearly 0.035 GPa as shown in Fig. 6(b).

The HCNFES process under a high *in situ* electrical poling and high-speed mechanical stretching can directly write the ultra-thin PVDF nanofibers with smooth surface morphology without unsteady solution flow rate in electrospinning. Therefore, under a strong mechanical alignment mechanism, the interface polymer chains in the vicinity of MWCNTs would be easily to form more compact packing of extended-chain crystallites along the fiber axis. In comparison of the NFES bare PVDF nanofibers and composite nanofibers, it is clear that the HCNFES PVDF/MWCNTs nanofibers
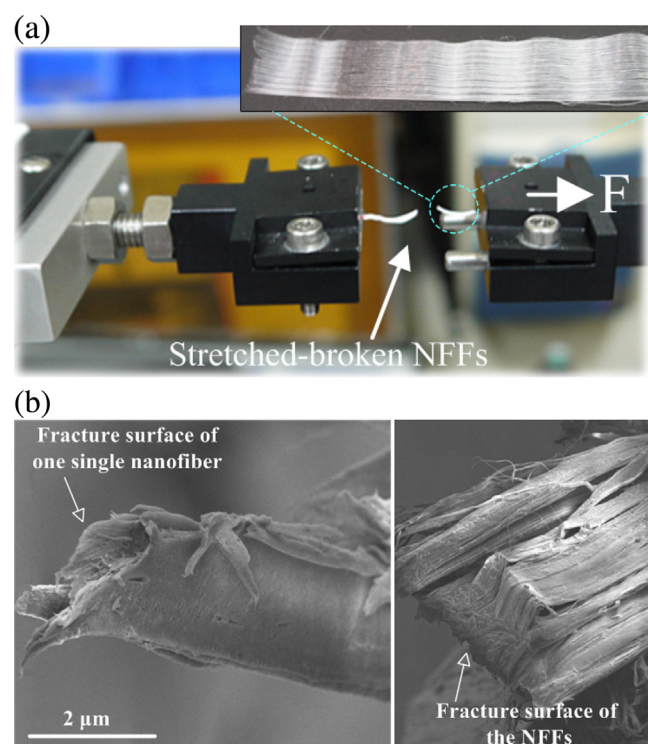
with high nucleation of the oriented β-form extended-chain crystallites can perform enhancement in mechanical properties and piezoelectricity.

3.2. Tensile testing

A direct tension test is well known as the most effective method to characterize the mechanical properties of electrospun fibers, such as yield stress, yield strain, ultimate tensile strength, and strain at break, that involve measuring applied axial force and fibers elongation under a known cross-sectional area. The tester MTS Tytron™ 250 microforce testing system was used. This highly accurate tester is used to be ideal for low-force static and dynamic mechanical testing of fibers. It has a load test capability at a range of 0.001–250 N with a load resolution of less than 1 mN. The extension resolution is in the range of 300 nm. The velocity of the moving head is adjusted at 0.12 mm/s to stretch the NFFs at a constant loading rate. To prepare the standard samples, the number of nanofibers can be controlled by the electrospinning processes, and the thickness and areal density are at ranges of ~10 μm and ~155 nanofibers/mm², respectively. The cross-sectional area of the NFFs in the range of ~1950 × 10^{-12} m² is evaluated from the whole parallel nanofiber arrays measured by SEM images. Finally, the NFFs both ends tightly bonded to the grip of a 15 mm gage length. Fig. 7(a) shows the schematic diagram of deformation of the electrospun NFFs after tensile test. An understanding of ductile failure surface of the electrospun nanofiber after the tensile test is shown in Fig. 7(b), and local failures are not observed on the failure surface. Fig. 8(a) shows the plotted force–elongation curves of the HCNFES composite NFFs with 16 wt% PVDF solution and 0.03 wt% MWCNTs. It can be seen that the axial force and elongation are 0.059 kgf (0.578 N), and 4.54 mm, respectively. Fig. 8(b) shows the force–elongation curves of the NFES composite NFFs. The axial force and elongation are 0.0699 kgf (0.686 N), and 3.97 mm, respectively.
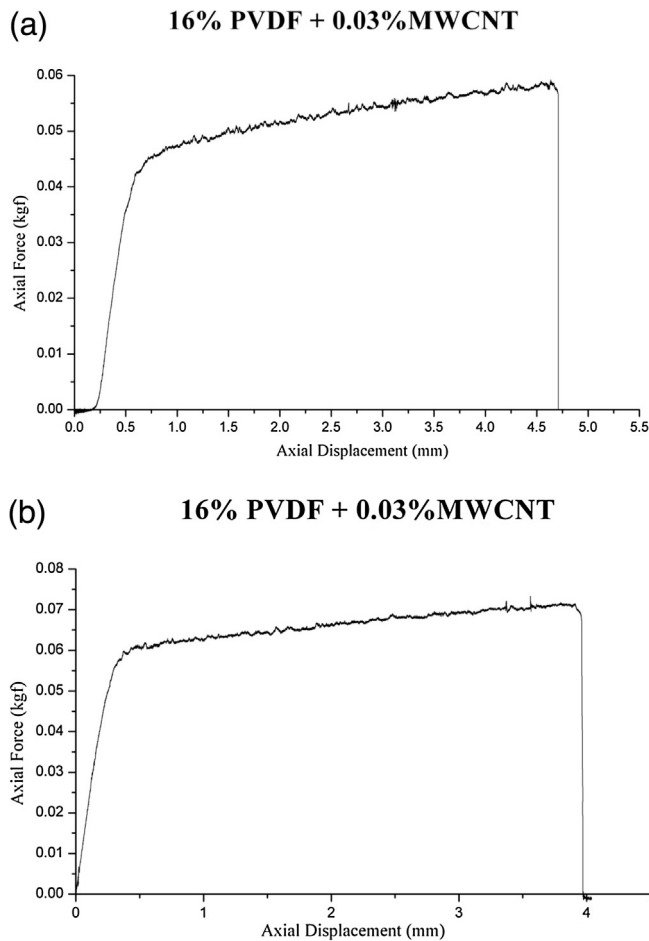
(a)

16% PVDF + 0.03%MWCNT

(b)

16% PVDF + 0.03%MWCNT

Fig. 8. The force–elongation curves of the NFFs with 16 wt% PVDF solution and 0.03 wt% MWCNTs: (a) by the HCNFES process and (b) by the NFES processes.

(a)

16% PVDF + 0.03%MWCNT

(b)

16% PVDF + 0.03%MWCNT

Fig. 9. The stress–strain curves of the NFFs with 16 wt% PVDF solution and 0.03 wt% MWCNTs: (a) by the HCNFES process and (b) by the NFES processes.

When the NFFs were stretched, the initial part of these curves shows that it went through a linear elasticity within a small range of strain with a high resistance to deformation. The possible reasons for such high resistance are the slightly entanglement of the nanofibers and the cohesive forces in the nanofibers assembly such that the nanofiber arrays could resist slippage and deformation [38,39]. In addition, after a long period of nanofiber collection in the HCNFES process, there could be slightly randomness on the NFFs surface caused by the presence of residual charges on the electrospun fibers, which leads to the mentioned phenomenon of fiber entanglement each other [40]. Further increases in axial force (strain) leaded to decreases in cross section of the test specimen and thus followed by nonlinear elasticity until the final breakage point is reached at the ultimate strain. The axial force is divided by the cross-sectional area of NFFs to obtain the stress (MPa). The strain (%) is obtained by dividing the elongation by the gauge length. Fig. 9(a) shows stress–strain curves of the HCNFES composite NFFs, which is rearranged by the axial force, cross-sectional area and elongation. The results show that the mechanical properties of the HCNFES composite NFFs are: tensile strength of 48.17 MPa, yield stress of 28 MPa, yield strain of 3.3% and strain at break of 32.5%. A yield stress point can be observed at the initial linear portion of the curves, followed by a gradual reduction in stress–strain ratio due to the initiative fiber slippage which leads to a slow increase in stresses. After further increases in stretching, the cross-sectional area of NFFs decreased, and resulted in a subsequent failure of the NFFs. Fig. 9(b) shows the plotted stress–strain curves of the NFES composite NFFs, which reveal the tensile strength of 45.71 MPa,
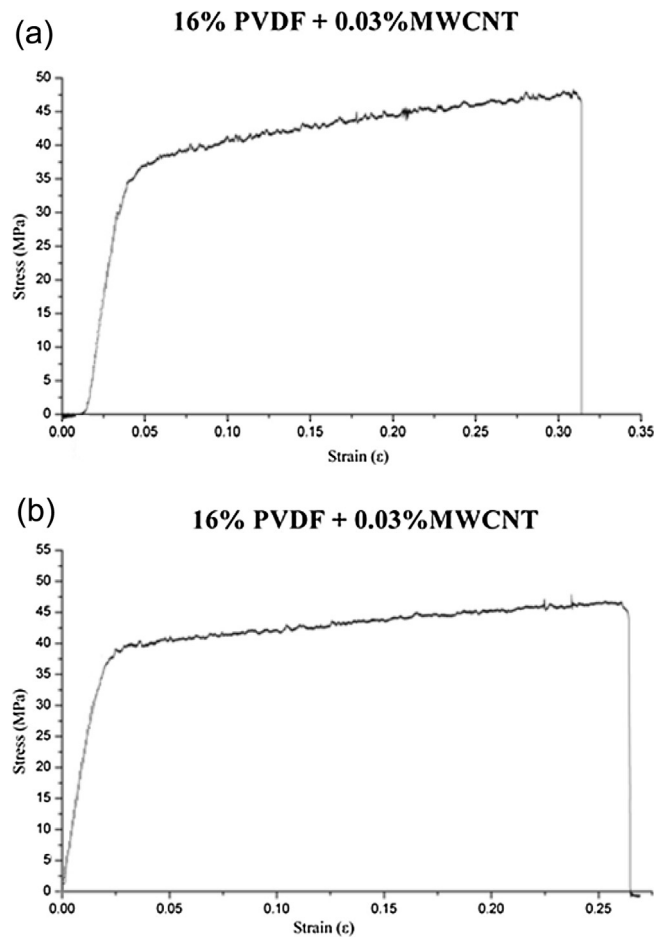
yield stress of 23.75 MPa, yield strain of 1.25%, and strain at break of 26.25%. Table 3 shows the characterization of the tensile NFFs under various solutions.

In the comparison of the FFES PVDF nanofiber mats [12], the remarkable improvement in mechanical properties of the HCN-FES PVDF nanofibers is owing to the high nucleation of oriented
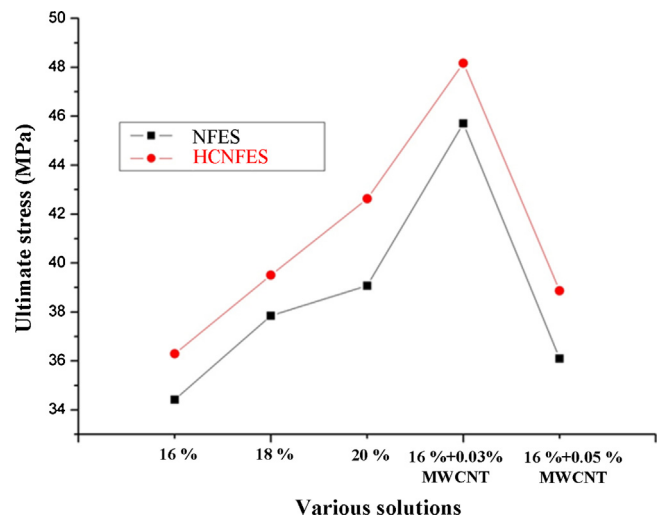

Fig. 10. The maximum tensile strength of the NFFs with various solutions via the HCNFES and the NFES processes.
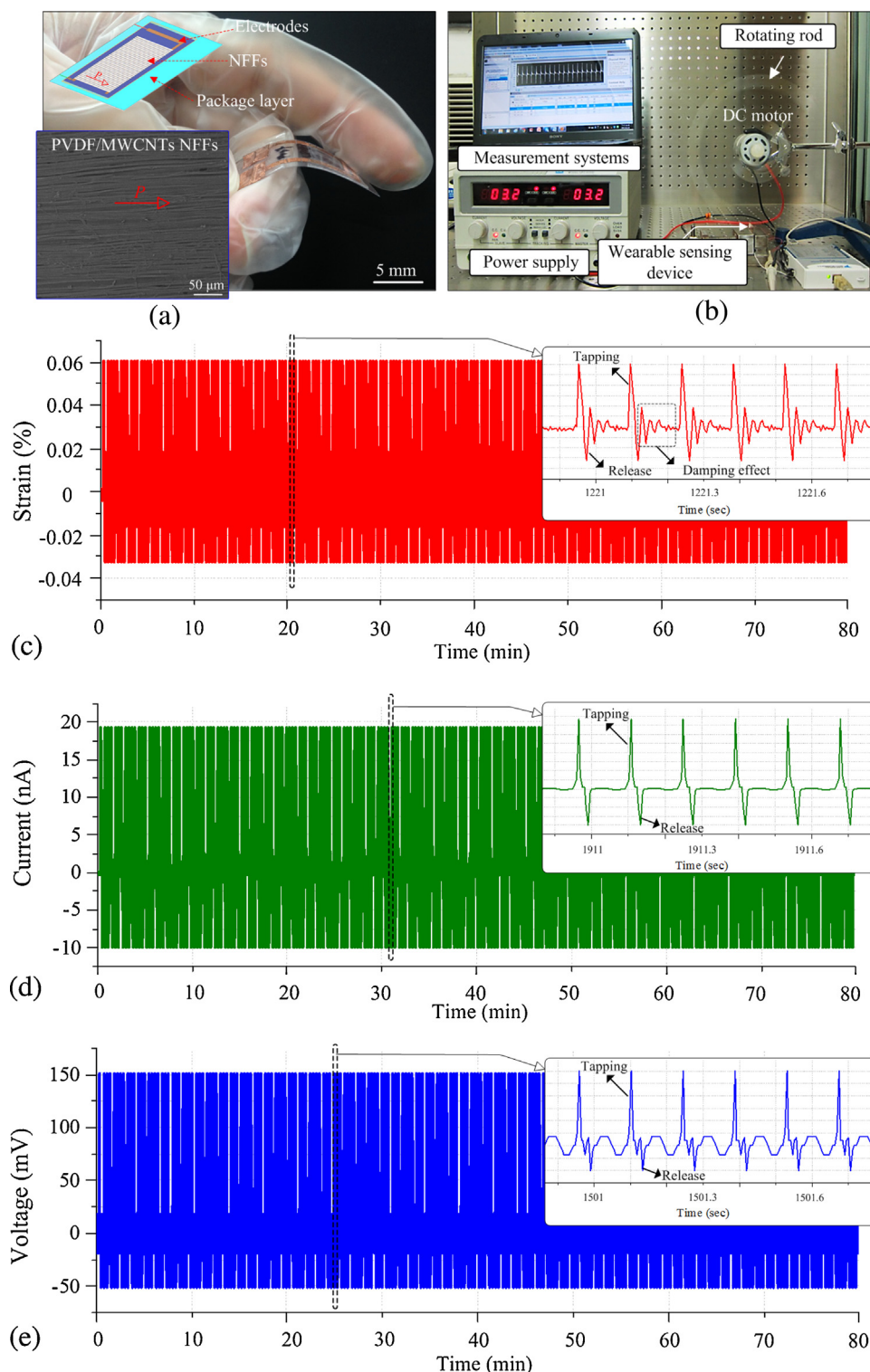
Fig. 11. (a) PVDF/MWCNTs NFFs fabricated by the HCNFES process with an optimal parameter of 16 wt% PVDF + 0.03 wt% MWCNTs is understood with average individual fiber diameter of ~2.5 μm for more than 10,000 fibers in parallel connection, (b) schematic diagram of the measurement system including a flexible wearable sensing device. Long-term stability tests and (c) plots of measured strains and (d and e) output voltages and currents under 6 Hz of continuous tapping-release for 80 min, revealing the stability. The insets show the detailed profiles of the electrical outputs.

extended-chain crystallites along the fiber axis in the electrospun nanofibers, which can be achieved by the strong alignment mechanism in the HCNFES process [41,42]. Further alignment of the PVDF nanofibers is necessary to attain the required mechanical properties and piezoelectricity. After adding MWCNTs to the PVDF NFFs, the improvement in mechanical properties and tensile strength is performed as shown in Fig. 10. We suggested that the interactions between MWCNTs and PVDF polymer crystallites could facilitate the nucleation of high oriented extended-chain crystallites in the HCNFES nanofibers [27,43]. However, when MWCNTs in PVDF solution exceeds 0.05 wt%, the electrospun nanofibers would exhibit lots of defects on the surface, leading to a poor crystallization in the

Table 3
Experimental data of tensile tests with various solutions, including axial force, elongation, and ultimate stress at break (note: HCNFES process (H); NFES (N)).

Concentration	Axial force (N)	Elongation (mm)	Ultimate stress (MPa)
H 16 wt%	0.479	3.27	36.29
H 18 wt%	0.442	3.45	39.51
H 20 wt%	0.213	3.88	42.63
H 16 wt% + 0.03 wt% MWCNTs	0.578	3.95	48.17
H 16 wt% + 0.05 wt% MWCNTs	0.253	1.89	38.87
N 16 wt%	0.229	2.89	34.42
N 18 wt%	0.455	3.45	37.85
N 20 wt%	0.215	3.54	39.08
N 16 wt% + 0.03 wt% MWCNTs	0.686	3.97	45.71
N 16 wt% + 0.05 wt% MWCNTs	0.470	1.89	36.10

PVDF nanofibers due to the worse orientation of molecular chains and the agglomeration effect of MWCNTs. These phenomena have also been confirmed by the nano-indentation tests, SEM results and XRD patterns.

3.3. Lifetime testing results of the PVDF/MWCNTs NFFs

Wearable sensor technology continues to advance and provide significant opportunities for improving personalized healthcare [44]. This study has manufactured a prototype of flexible wearable sensor device that is expected to be light-weight, highly durable, flexible, and conformable, which may monitor movement, medical physiology and environment for further applications in protection from exercise injuries and long-term care. The electrospun PVDF/MWCNTs NFFs exhibited better mechanical and electrical properties in the aligned direction [45,46]. After electrospun the orderly piezoelectric NFFs with a thickness of ~10 μm on a thin polymer substrate (50 μm) and with both ends tightly bonded to two electrodes, the entire structure was packaged to maintain its physical stability (Fig. 11(a)). The measurement apparatuses are shown in Fig. 11(b). The long-term stability of the wearable sensing device was examined through operation over an extended period of low-frequency mechanical tapping to bend the flexible polymer structure for 80 min. When an axial stress is applied in the piezoelectric active layer of the PVDF/MWCNTs NFFs, a piezoelectric potential is generated. After tapping and releasing processes, alternating voltage and current can be generated via the transverse mode piezoelectric effect and variation of the axial strains was also recorded by the strain gauges. The wearable sensing device generated an average voltage of ~200 mV$_{p-p}$ (V_{max} = ~150 mV) and current of ~30 nA$_{p-p}$ (I_{max} = ~20 nA) upon receiving a 6 Hz mechanical vibration with a maximum tensile strain of 0.06% and the electrical outputs are relatively stable without noticeable degradation as shown in Fig. 11(c–e). In addition, the insets show the detailed profiles of the axial strains and electrical outputs, and the tapping process results in a higher strain rate that dominates electrical outputs more than the releasing process about 2–3 times.

4. Conclusions

A continuously HCNFES technique to obtain well-aligned self-assembled PVDF NFFs with a small amount of added MWCNTs can be carried out. Upon aligning the nanofibers, we aim to mechanically characterize the HCNFES and NFES PVDF NFFs via nano-indentation and microtensile tests to perform an assessment of the average mechanical properties. The HCNFES process combines electrical poling and high uniaxial stretching in one-single step, SEM and XRD results show that the high density NFFs with smaller diameter, smooth surface and highly nucleation of the oriented β-form extended-chain crystallites along the fiber axis can be quickly formed. A noticeable effect on the mechanical properties and piezoelectricity of the HCNFES PVDF/MWCNTs NFFs

suggested that the interfacial interaction between the interface PVDF chains and MWCNTs can facilitate the higher nucleation of β-form extended-chain crystallites. Such the HCNFES PVDF/MWCNTs NFFs with improved strength and β-crystalline phase content can be useful for energy transducers and electromechanical actuators, and combine them into more complex circuits as well as functional nanowire clothes.

References

[1] X. Chen, S.Y. Xu, N. Yao, 1.6 V nanogenerator for mechanical energy harvesting using PZT nanofibers, Nano Lett. 10 (2010) 2133–2137.
[2] Y. Qi, N.T. Jafferis, K. Lyons Jr., C.M. Lee, H. Ahmad, M.C. McAlpine, Piezoelectric ribbons printed onto rubber for flexible energy conversion, Nano Lett. 10 (2010) 524–528.
[3] X. Chen, S. Xu, N. Yao, W. Xu, Y. Shi, Potential measurement from a single lead ziroconate titanate nanofiber using a nanomanipulator, Appl. Phys. Lett. 94 (2009) 253113.
[4] G. Zhang, S. Xu, Y. Shi, Electromechanical coupling of lead zirconate titanate nanofibres, Micro Nano Lett. 6 (2011) 59–61.
[5] G. Zhu, R.S. Yang, S.H. Wang, Z.L. Wang, Flexible high-output nanogenerator based on lateral ZnO nanowire array, Nano Lett. 10 (2010) 3151–3155.
[6] Z.L. Wang, J. Song, Piezoelectric nanogenerators based on zinc oxide nanowire arrays, Science 312 (2006) 242–246.
[7] Y. Qin, X. Wang, Z.L. Wang, Microfibre-nanowire hybrid structure for energy scavenging, Nature 451 (2008) 809–813.
[8] R. Yang, Y. Qin, L. Dai, Z.L. Wang, Power generation with laterally packaged piezoelectric fine wires, Nat. Nanotechnol. 4 (2008) 34–39.
[9] S.N. Cha, J.S. Seo, S.M. Kim, H.J. Kim, Y.J. Park, S.W. Kim, Sound-driven piezoelectric nanowire-based nanogenerators, Adv. Mater. 22 (2010) 4726–4730.
[10] J. Chang, M. Dommer, C. Chang, L.W. Lin, Piezoelectric nanofibers for energy scavenging applications, Nano Energy 1 (3) (2012) 356–371.
[11] Z.H. Liu, C.T. Pan, L.W. Lin, H.W. Lai, Piezoelectric properties of PVDF/MWCNT nanofiber using near-field electrospinning, Sensors Actuat. A: Phys. 193 (2012) 13–24.
[12] H. Yu, T. Huang, M. Lu, M. Mao, Q. Zhang, H. Wang, Enhanced power output of an electrospun PVDF/MWCNTs-based nanogenerator by tuning its conductivity, Nanotechnology 24 (40) (2013) 405401.
[13] D. Sun, C. Chang, S. Li, L.W. Lin, Near-field electrospinning, Nano Lett. 6 (4) (2006) 839–842.
[14] S. Vidhate, A. Shaito, J. Chung, N.A. D'Souza1, Crystallization, mechanical, and rheological behavior of polyvinylidene fluoride/carbon nanofiber composites, Appl. Polym. Sci. 112 (2009) 254–260.
[15] B. Mohammadi, A.A. Yousefi, S.M. Bellah, Effect of tensile strain rate and elongation on crystalline structure and piezoelectric properties of PVDF thin films, Polym. Test. 26 (2007) 42–50.
[16] J.S. Nunes, V. Sencadas, A. Wu, A.L. Kholkin, P.M. Vilarinho, S. Lanceros-Me'ndez, Mater. Res. Soc. Symp. Proc. 949 (2007), 0949-C03-02.
[17] A.J. Lovinger, D.C. Bassett, Developments in Crystalline Polymers, Applied Science Publishers, London, 1982 (Chapter 5).
[18] A.J. Lovinger, Ferroelectric polymers, Science 220 (1983) 1115–1121.

[19] F. Schaffner, B.J. Jungnickel, The electric moment contribution to the piezoelectricity of PVDF, IEEE Trans. Dielectr. Electr. Insul. 1 (1994) 553–562.

[20] W.A. Yee, M. Kotaki, Y. Liu, X. Lu, Morphology, polymorphism behavior and molecular orientation of electrospun poly(vinylidene fluoride) fibers, Polymer 48 (2) (2007) 512–521.

[21] D.H. Reneker, A.L. Yarin, H. Fong, S. Koombhongse, Bending instability of electrically charged liquid jets of polymer solutions in electrospinning, J. Appl. Phys. 87 (9) (2000) 4531–4547.

[22] C. Chang, K. Limkrailassiri, L.W. Lin, Continuous near-field electrospinning for large area deposition of orderly nanofiber patterns, Appl. Phys. Lett. 93 (12) (2008) 123111.

[23] C. Chang, V.H. Tran, J. Wang, Y.K. Fuh, L.W. Lin, Direct-write piezoelectric polymeric nanogenerator with high energy conversion efficiency, Nano Lett. 10 (2010) 726–731.

[24] Z.H. Liu, C.T. Pan, L.W. Lin, J.C. Huang, Z.Y. Ou, Direct-write PVDF nonwoven fiber fabrics energy harvesters via the hollow cylindrical near-field electrospinning process, Smart Mater. Struct. 23 (2014) 025003.

[25] S.Y. Gu, Q.L. Wu, J. Ren, G.J. Vancso, Mechanical properties of a single electrospun fiber and its structures, Macromol. Rapid Commun. 26 (2005) 716–720.

[26] C. Tang, H. Liu, Cellulose nanofiber reinforced poly(vinyl alcohol) composite film with high visible light transmittance, Compos. Part A 39 (2008) 1638–1643.

[27] S. Huang, W.A. Yee, W.C. Tjiu, Y. Liu, M. Kotaki, Y.C.F. Boey, J. Ma, T. Liu, X. Lu, Electrospinning of polyvinylidene difluoride with carbon nanotubes: synergistic effects of extensional force and interfacial interaction on crystalline structures, Langmuir 24 (23) (2008) 13621–13626.

[28] A. Baji, Y.W. Mai, Q. Li, Y. Liu, Electrospinning induced ferroelectricity in poly(vinylidene fluoride) fibers, Nanoscale 3 (2011) 3068–3071.

[29] X. Ren, Y. Dzenis, Novel continuous poly(vinylidene fluoride) nanofibers, Mater. Res. Soc. Symp. Proc. 920 (2006), 0920-S03-03.

[30] T. Miyata, T. Masuko, Crystallization behavior of poly(ʟ-lactide), Polymer 39 (1998) 5515–5521.

[31] B. Na, N. Tian, R. Lv, Z. Li, W. Xu, Q. Fu, Evidence of sequential ordering during cold crystallization of poly(ʟ-lactide), Polymer 51 (2010) 563–567.

[32] N.K. Singh, S.K. Singh, D. Dash, P. Gonugunta, M. Misra, P. Maiti, CNT induced β-phase in polylactide: unique crystallization, biodegradation, and biocompatibility, Phys. Chem. C 117 (2013) 10163–10174.

[33] Y. Liu, S. Kumar, Polymer/carbon nanotube nano composite fibers – a review, ACS Appl. Mater. Interfaces 6 (9) (2014) 6069–6087.

[34] Y.L. Lin, Z.H. Liu, C.T. Pan, L.W. Lin, W.C. Wang, F.T. Hsu, Z.Y. Ou, Characteristic of single-fiber PVDF nanoharvester via new hollow cylindrical near-field electrospinning process, in: 17th International Solid-State Sensors, Actuators and Microsystems Conference (Transducers'13), Barcelona, Spain, June 16–20, 2013.

[35] J.L. Loubet, B.N. Lucas, W.C. Oliver, Some measurements of viscoelastic properties with the help of nanoindentation, in: Proc. of the International Workshop on Instrumental Indentation, 1995, pp. 31–34.

[36] C.T. Lim, E.P.S. Tan, S.Y. Ng, Effects of crystalline morphology on the tensile properties of electrospun polymer nanofibers, Appl. Phys. Lett. 92 (14) (2008) 141908-1–141908-3.

[37] B.J. Briscoe, A. Akram, M.J. Adams, S.A. Johnson, D.M. Gorman, The influence of solvent quality on the mechanical properties of thin cast isotactic poly(methyl methacrylate) coatings, J. Mater. Sci. 37 (2002) 4929–4936.

[38] J. Ayutsede, M. Gandhi, S. Sukigara, M. Micklus, H.E. Chen, F. Ko, Regeneration of *Bombyx mori* silk by electrospinning. Part 3: characterization of electrospun nonwoven mat, Polymer 46 (5) (2005) 1625–1634.

[39] M.B. Bazbouz, G.K. Stylios, The tensile properties of electrospun Nylon 6 single nanofibers, J. Polym. Sci. B: Polym. Phys. 48 (15) (2010) 1719–1731.

[40] W.A. Yee, M. Kotaki, Y. Liu, X. Lu, Morphology polymorphism behavior and molecular orientation of electrospun poly(vinylidene fluoride) fibers, Polymer 48 (2) (2007) 512–521.

[41] M.B. Bazbouz, G.K. Stylios, Alignment and optimization of nylon 6 nanofibers by electrospinning, J. Appl. Polym. Sci. 107 (5) (2008) 3023–3032.

[42] M.V. Jose, B.W. Steinert, V. Thomas, D.R. Dean, M.A. Abdalla, G. Price, G.M. Janowski, Morphology and mechanical properties of Nylon 6/MWNT nanofibers, Polymer 48 (4) (2007) 1096–1104.

[43] N.K. Singh, S.K. Singh, D. Dash, P. Gonugunta, M. Misra, P. Maiti, CNT induced β-phase in polylactide: unique crystallization, biodegradation, and biocompatibility, J. Phys. Chem. C 117 (19) (2013) 10163–10174.

[44] M.M. Rodgers, V.M. Pai, R.S. Conroy, Recent advances in wearable sensors for health monitoring, Sensors J. IEEE (99) (2014).

[45] G.Y. Gu, Z.J. Wang, D.J. Kwon, J.M. Park, Mechanical and electrical properties of electrospun CNT/PVDF nanofiber for micro-actuator, Compos. Res. 26 (1) (2013) 14–20.

[46] H. Ye, H. Lam, N. Titchenal, Y. Gogotsi, F. Ko, Reinforcement and rupture behavior of carbon nanotubes–polymer nanofibers, Appl. Phys. Lett. 85 (2004) 1775–1777.